

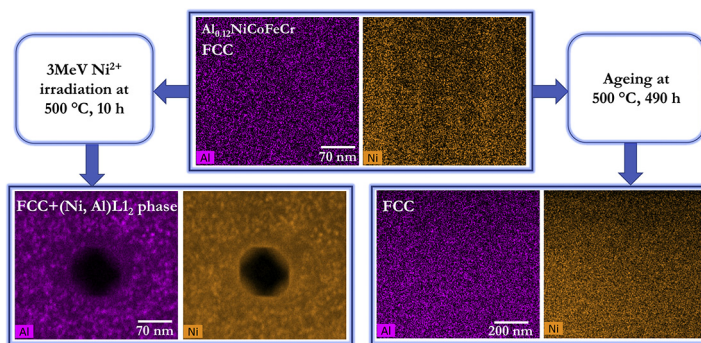
# Phase stability of single phase $\text{Al}_{0.12}\text{CrNiFeCo}$ high entropy alloy upon irradiation<sup>☆</sup>

B. Kombaiah\*, K. Jin, H. Bei, P.D. Edmondson, Y. Zhang

Materials Science and Technology Division, Oak Ridge National Laboratory, Oak Ridge, TN 37831, USA



## GRAPHICAL ABSTRACT



## ARTICLE INFO

### Article history:

Received 11 July 2018

Received in revised form 25 September 2018

Accepted 2 November 2018

Available online 6 November 2018

### Keywords:

Phase transformation

High entropy alloys

Irradiation

Alloy design

Electron microscopy

## ABSTRACT

Phase stability of  $\text{NiCoFeCr}$  and  $\text{Al}_{0.12}\text{NiCoFeCr}$  single phase high entropy alloys (HEAs) was studied under  $3\text{ MeV Ni}^{2+}$  irradiation at  $500\text{ }^{\circ}\text{C}$  to a fluence of  $1 \times 10^{17}/\text{cm}^2$  reaching a peak dose of  $\sim 100$  displacements per atom (dpa). Transmission electron microscopy (TEM) diffraction pattern and scanning transmission electron microscopy-energy dispersive X-Ray spectroscopy (STEM-EDS) were utilized to detect any second phases that formed in the irradiated regions of the specimens. While the single phase of  $\text{NiCoFeCr}$  alloy has remained stable under the irradiation, the phase in  $\text{Al}_{0.12}\text{NiCoFeCr}$  alloy decomposed into FCC matrix phase, and  $\text{Ni}_3\text{Al}$  type nanoprecipitates with  $\text{L1}_2$  ordered structure. On the other hand, in  $\text{Al}_{0.12}\text{NiCoFeCr}$  alloy, the non-irradiated region of the TEM specimen (annealed for  $10\text{ h}$  at  $500\text{ }^{\circ}\text{C}$ ) and the as-cast alloy annealed for  $490\text{ h}$  at  $500\text{ }^{\circ}\text{C}$  exhibited no such precipitates similar to those observed in the irradiated region. Based upon the thermodynamic stability of these alloys, we propose that radiation-enhanced diffusion under the irradiation accelerated the formation of the  $\text{Ni}_3\text{Al}$  type equilibrium phase. Our study clearly demonstrates that the phase stability of HEAs under irradiation should be considered as one of the deciding factors in the materials design and selection for nuclear applications.

© 2018 Elsevier Ltd. All rights reserved.

## 1. Introduction

Equi-atomic multicomponent concentrated solid-solution alloys (CSAs) or high entropy alloys (HEAs) are candidate structural materials for critical applications due to the combination of their excellent mechanical properties at a range of temperatures and excellent chemical properties and compatibilities [1–6]. It has recently been demonstrated that CSAs have a much higher tolerance to energetic particle radiation effects, such as resistance to void swelling and defect formation than

<sup>☆</sup> This manuscript has been authored by UT-Battelle, LLC, under contract DE-AC05-00OR22725 with the US Department of Energy (DOE). The US government retains and the publisher, by accepting the article for publication, acknowledges that the US government retains a nonexclusive, paid-up, irrevocable, worldwide license to publish or reproduce the published form of this manuscript, or allow others to do so, for US government purposes. DOE will provide public access to these results of federally sponsored research in accordance with the DOE Public Access Plan (<http://energy.gov/downloads/doe-public-access-plan>).

\* Corresponding author.

E-mail address: [bkombai@ncsu.edu](mailto:bkombai@ncsu.edu) (B. Kombaiah).

conventional alloys [7–9]. Such characteristics have been argued to arise partially from their intrinsic chemical disorder and lattice distortion [10] that causes higher defect formation barrier, slow atomic diffusion, and reduction in the thermal and electrical conductivities, leading to increased recombination of radiation-produced vacancies and interstitials [7,11,12]. For these reasons, CSAs, including HEAs, have been proposed as potential candidate materials for Generation IV and Fusion based nuclear reactors that operate at higher temperatures and irradiation doses than the present generation reactors [13–15]. One unique approach to further enhance the ability of modifying defect dynamics in CSAs is to add low concentration of dopants (e.g., elements from different group or period of the Periodic Table) to form doped-CSAs or doped-HEAs. While adding solutes to improve radiation resistance in diluted alloys is well demonstrated, combining the concepts of dilute and concentrated alloys to introduce deep sinks in CSAs/HEAs may further improving radiation tolerance.

One critical requirement for the application of materials in a radiation environment at elevated temperatures would be the resistance to the formation of undesirable phases during service that would result in detrimental properties. Formation of such secondary phases could either be induced or enhanced by the displacement cascade produced by radiation. For instance, Cr rich  $\alpha'$  phase formation in Cr steels that leads to embrittlement has been suggested to be enhanced by radiation damage via accelerated diffusion of elements [16–18]. An example for the radiation-induced precipitation much relevant to the nuclear technology would be the separation of Ni-rich and Si-rich phases or  $\gamma'$  phase ( $\text{Ni}_3\text{Si}$ ) in irradiated austenitic stainless steels that have not been detected in the thermally treated steels [19,20]. Other classic examples of radiation-induced precipitation (RIP) in undersaturated solid solutions are Ni-Si, Ni-Ge, and Ni-Be alloys, in which the Ni-rich precipitation has been found to occur at defect sinks where the solute concentration exceeds the solubility limit at the given temperature through radiation-induced segregation (RIS) [21,22]. Furthermore, the formation of Cu-rich and Ni-Mn-Si rich precipitates under neutron irradiation in reactor pressure vessel steels of light water reactors (LWR) is the life-limiting factor in the life extensions of the reactors due to their resulting embrittlement. While the Cu rich precipitates could form thermodynamically, the Ni-Mn-Si rich precipitates have been found to nucleate heterogeneously within the displacement cascades [23,24]. In Al-1.9% Zn undersaturated solid solutions, however, the radiation-induced Zn-rich phase has been observed to precipitate homogeneously throughout the matrix with no assistance from any RIS phenomena as described in the previous case [25]. Such precipitation has been argued to originate from the recombination of interstitials and vacancies during irradiation [26,27].

In this context, phase changes caused by radiation in HEAs and doped-HEAs have become a primary concern while considering that the desirable properties of HEAs are the resultant of the phase(s) achieved by choosing a suitable composition. Consequently, any changes in phase could potentially lead to detrimental properties like the formation of intermetallic phases in HEAs during ageing resulting in a precipitous loss in ductility and loss of corrosion resistance [28–31]. Therefore, it is critical to characterize and understand the phase stability of HEAs and doped-HEAs under severe irradiation conditions to qualify them for the applications in radiation environment. On the other hand, ion beam synthesis of nanoprecipitates in HEAs is open research field. Only a few studies focusing on the phase stability of HEAs, even less in doped-HEAs, under irradiation are available due to the relatively recent emergence of the field [12,32–35]. Inclusion of nanoprecipitates in HEAs may provide further desired properties, similarly as Oxide Dispersed Strengthened (ODS) steels, as structural materials for future large-scale energy facilities. Understanding formation mechanisms of precipitations in HEAs would contribute to assessments of their economic impact for industrialization.

On investigating the phase stability of high entropy alloys under irradiation conditions, Kiran Kumar et al. detected no phase separation

in the 3 or 5.8 MeV Ni ion irradiated a non-equiautomic FeNiCrMn alloy in doses ranging from 0.03 to 10 displacements per atom (dpa) at the temperature range of room temperature to 700 °C, demonstrating the phase stability of the HEA under the irradiation conditions [32]. Similarly,  $\text{Al}_x\text{CoCrFeNi}$  ( $x = 0.1, 0.75$  and  $1.5$  M ratios) alloys maintained their original phase(s) following the irradiation of the TEM thin foils with 3MeV Au ions at room temperature to induce maximum doses of about 100 dpa in the studies by Xia et al. and Yang et al. demonstrating the phase stability of these alloys[12–33]. It should be underscored that the room temperature irradiation experiments conducted in these studies would exclude any thermally assisted diffusion processes that could accelerate the phase transformations having thermodynamic feasibility [36]. Recently,  $\text{Al}_{0.1}\text{CoCrFeNi}$  alloy with single phase has been shown to have phase stability even at high temperature irradiation experiments conducted at the range of 250–650 °C with 3 MeV Au ions resulting in a peak dose of 31 dpa [37]. In the preceding cases, high entropy configurations and slow diffusion owing to compositional complexity were postulated as the reasons behind the phase stability of the alloys. On the other hand, some other HEAs have been observed to form second phases under a different set of irradiation conditions. For instance, equiautomic CrFeCoNiMn and CrFeCoNiPd alloys were found to produce L10 (NiMn) phase and undergo spinoidal decomposition between Cr/Ni and Pd rich phases, respectively, after 1250 eV electron irradiation up to a dose of 1 dpa at about 400 °C [34]. Here, it was argued that the enthalpy of mixing between individual elements in the alloys primarily governed the kind of phases separating from the original phase during irradiation. In the case of CrFeCoNiMn alloy, as an example, the separation NiMn phase was ascribed to a high negative enthalpy of mixing between Ni and Mn ( $-8$  to  $-11$  kJ/mol).

This study aims to probe the phase stability under ion irradiation of two important alloys: NiCoFeCr HEA and Al doped HEA ( $\text{Al}_{0.12}\text{NiCoFeCr}$  where 0.12 denotes the mole fraction of Al in the alloy). These HEAs are considered for structural materials at high temperatures, including nuclear reactors, due to their exceptional mechanical and chemical properties [38–40]. Both of the HEAs have been shown to maintain their original phases under the ion irradiation up to doses of ~50 dpa and ~30 dpa respectively at high temperatures [35,37]. In this work, the phase stability of NiCoFeCr and  $\text{Al}_{0.12}\text{NiCoFeCr}$  HEAs was investigated after subjecting them to more severe Ni ion irradiation with a peak dose reaching ~100 dpa at a temperature of 500 °C. Such a high dose irradiation condition is relevant to the structural materials in the future reactor designs that can experience a dose level in excess of 100 dpa [41].

## 2. Materials and experiments

In this work, single phase HEAs, equiautomic NiCoFeCr and NiCoFeCr alloy doped with 3 at.% Al in as-cast condition were used. To produce these alloys, the elemental metals Ni, Co, Fe, Cr, and Al (>99.9% pure) were carefully weighed and mixed by arc melting, based on the designed compositions. The arc-melted buttons were flipped and remelted at least five times before drop casting to ensure homogeneous mixing. In order to achieve large grain sizes to minimize the effect of grain boundaries, the specimens were rolled at room temperature in steps to a final thickness of ~1.8 mm, and then annealed at 1200 °C for several days. The average grain size of these alloys is approximately 250  $\mu\text{m}$ . The alloys were then chemically-mechanically polished using colloidal silica to a surface roughness below 3 nm. The samples of size about 5 mm  $\times$  5 mm  $\times$  1 mm were irradiated with 3 MeV  $\text{Ni}^{2+}$  at 500 °C to a fluence of  $1 \times 10^{17}/\text{cm}^2$  at a beam flux of approximately  $2.8 \times 10^{12}$  ions/ $\text{cm}^2/\text{s}$ , accounting for about 10 h of irradiation time. The Ni beam was defocused to have a broad profile and wobbled over the irradiated area to ensure uniform irradiation with scanning frequencies of 517 and 64 Hz for the horizontal and vertical direction, respectively [42].

The irradiation-induced damage profile and Ni concentration were predicted using the Stopping and Range of Ions in Matter (SRIM)

program by choosing the calculation type 'Ion distribution and quick calculation of damage' [43,44]. In the calculations, the target was irradiated with 3 MeV Ni ions. The target composition was set to be consisting of Ni, Co, Fe and Cr in equal measures and the density of the target was assumed to be 8 g/cm<sup>3</sup>. Likewise, a value of 40 eV was set for the displacement threshold energy [7]. A total count of 10<sup>5</sup> ions was included in the SRIM calculations. The damage profile, in terms of displacements per atom (dpa), was determined from the sum of the total number of vacancies (produced by the Ni ions and Fe, Co, Ni and Cr recoils) and the replacement collisions, whereas the software directly provided the Ni concentration profile.

Transmission Electron Microscope (TEM) thin foils were prepared by applying a Focused Ion Beam (FIB) technique using a FEI Quanta 3D 200i dual-beam Scanning Electron Microscope (SEM) and FIB system. Subsequently, to minimize the surface damage induced by the FIB sectioning, the thin foil was polished with low energy (900 eV and 600 eV) Ar ions using a model 1040 Fishione nanomill. For microstructural characterization, a JEOL JEM 2010F TEM and a FEI Talos F200X Scanning Transmission Electron Microscope (STEM) were employed. STEM-Energy Dispersive Spectroscopy (EDS) – compositional mapping was conducted using the FEI microscope, which is equipped with a Super-X energy dispersive spectrometer system, offering high quality compositional mapping with a high elemental detection limit. The compositional data was collected as EDS-X-Ray count maps, from which Quantity maps (Q-maps) were calculated using the Espirit-Bruker software by applying the Cliff-Lorimer method for further analysis [45].

### 3. Results

Under-focused bright-field TEM images exhibiting voids in NiCoFeCr and Al<sub>0.12</sub>NiCoFeCr tested in this study are given in Fig. 1. As seen from the figure, the irradiation cascade produced a distribution of voids in the irradiated regions of the materials. The size distribution and number density of the voids are similar between the two alloys. Also, provided for comparison are the dose and Ni concentration profiles along the depth as obtained using the SRIM software for the specified irradiation conditions. According to the profiles, a maximum dose of ~100 dpa

occurs at a depth of ~1 μm, and a peak Ni concentration of ~2.0 at. % is present at a slightly larger depth of ~1.2 μm.

#### 3.1. Phase stability

In the as-processed condition, these alloys had single solid solution phase with a homogenized composition of the constituents. During irradiation, due to the applied temperature or the damage cascade created by the ion irradiation or both, precipitation of new phases could occur. It should be noted that the effect on the grain boundaries on the radiation damage phenomena is negated owing to the large grain size in these alloys. To detect any second phases resulting from irradiation, selected area diffraction patterns and STEM-EDS maps obtained from the irradiated region of the alloys were taken.

In NiCoFeCr alloy, no extra diffraction points apart from those arising from the FCC matrix were noted and, correspondingly, no second phases were observed from the STEM-EDS maps as given in Fig. 2. Also, the EDS maps revealed no chemical inhomogeneity in the matrix apart from the RIS at the voids, underscoring the excellent stability of the parent phase of the alloy under the irradiation conditions. At the edge of the voids, Ni and Co were enriched, and Cr, Fe were depleted as noted from the EDS maps due to RIS.

On the other hand, in the irradiated region of Al<sub>0.12</sub>NiCoFeCr alloy, extra diffraction points apart from that arising from the FCC matrix were visible indicating new phase formation there (Fig. 3a). Dark-field imaging selecting only the electrons contributing to the extra diffraction point revealed the second phase as nanometer-sized precipitates distributed in the irradiated region (Fig. 3b). Using the dark-field images, the sizes of around 160 precipitates in the irradiated region were measured using the Image J software. The size distribution of the precipitates is provided in Fig. 3c with an average size of about 9 nm. It was noted that the sizes of the precipitate showed no notable dependency on the irradiation depth with the dose increased 40 dpa–100 dpa. Assuming that the average thickness of the TEM specimen was about 100 nm, the volume fraction of the precipitates was calculated to be about 9%.

STEM-EDS maps revealed the fine precipitates as enriched in Ni and Al in the irradiated region as given in Fig. 4. Furthermore, Fig. 4g shows

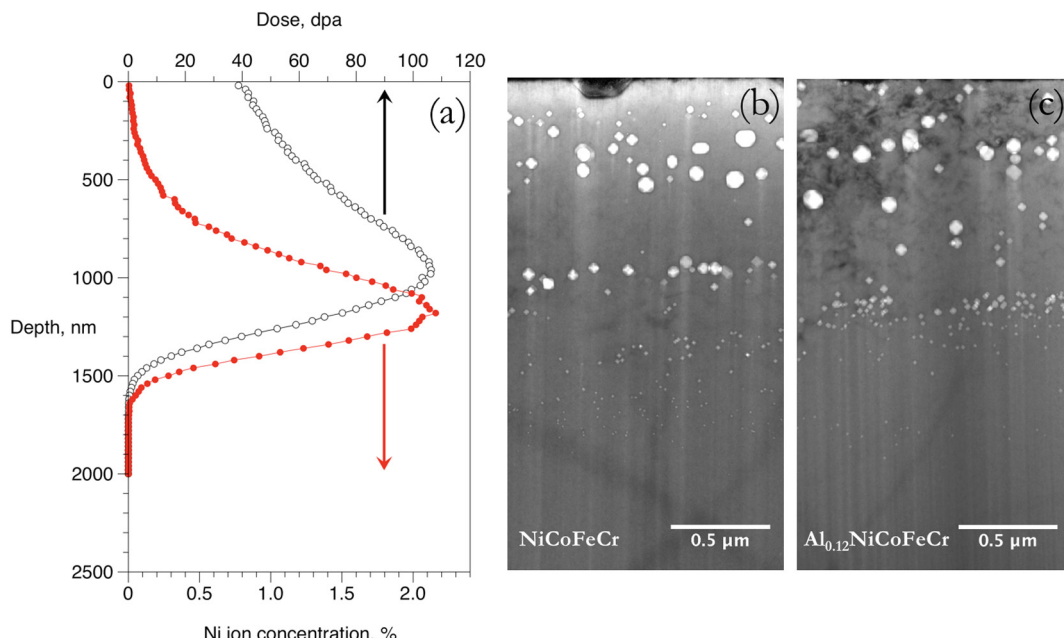


**Fig. 1.** a) Dose and Ni concentration profile along the depth calculated using the SRIM software for 3 MeV Ni ion irradiation of NiCoFeCr target to a fluence of  $1 \times 10^{17}/\text{cm}^2$ . b) and c) Bright-field TEM images recorded in an under-focused condition showing the distribution of voids along the irradiation depth in NiCoFeCr and Al<sub>0.12</sub>NiCoFeCr, respectively. These images were taken after tilting the specimens out of diffraction contrast to see the voids clearly and therefore the defects present in the materials stay invisible.

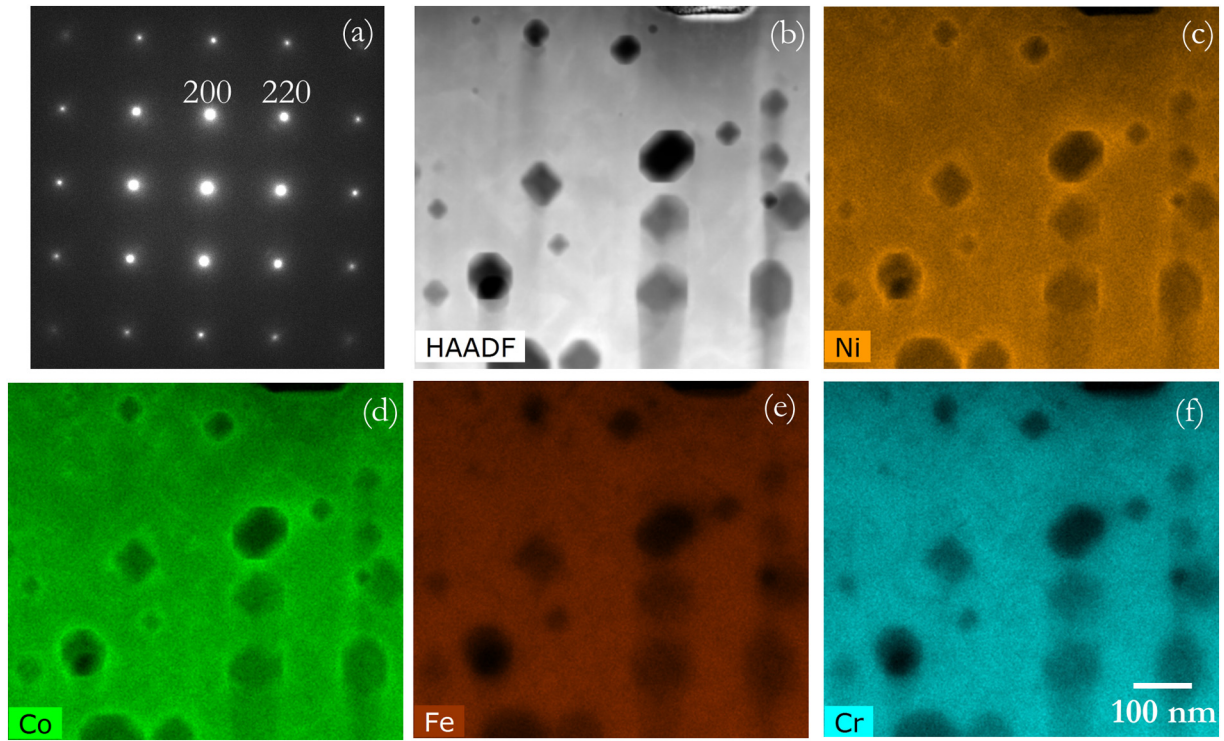


**Fig. 2.** In NiCoFeCr alloy, (a) [001] zone axis selected area diffraction pattern obtained from the irradiated region (b) STEM-HAADF image showing voids in the irradiation depth range of 0.1–0.7  $\mu\text{m}$  corresponding to the dose range of 40–90 dpa, (c–f) EDS-count maps of elements Ni, Co, Fe and Cr. The scale bar in (f) is applicable to (b–f).

the Ni and Al concentrations extracted from 20 regions of quantity maps each having the precipitates and the matrix, and it can be seen that both Ni and Al are enriched in the precipitate regions compared to the matrix, as evident from the count maps. Since the average size of the precipitates (~9 nm) is much smaller than a typical TEM specimen thickness (~100 nm), the composition extracted from the precipitate regions does not represent the exact composition of these precipitates. Such analysis, however, could only indicate the elements of which the precipitates are primarily composed and doesn't exclude the possibility of other elements such as Fe, Cr, and Co being present in the precipitates.

Based on our knowledge that these precipitates are primarily composed of Ni and Al, and the geometry of the extra points appeared in the diffraction point, the second phase precipitates were identified with Ni<sub>3</sub>Al type phase with L1<sub>2</sub> crystal structure as shown in Fig. 3. Another striking observation from the juxtaposition of the Al-EDS map with the MAADF (Medium Angle Annular Dark Field) image showing

voids was the precipitates-denuded zone around the voids, where the density of the precipitates is significantly low (Fig. 5). Such denuded zones were observable by its mere contrast due to its reduced precipitate number density in comparison to that in the matrix region and were measured to extend up to a distance of 40 nm from the edges of the voids (Fig. 5b). Excluding the precipitate denuded zone around the voids, a high number density of the precipitates was present in the irradiated region till a depth of 1050 nm beyond which the density abruptly falls close to zero. In other words, no precipitates were observed in the non-irradiated region of the TEM specimen.

#### 4. Discussion

Both NiCoFeCr and Al<sub>0.12</sub>NiCoFeCr HEAs exhibited single phase solid solution with FCC crystal structures, which is consistent with the earlier observations in similar alloys [12]. Our post-irradiation characterization

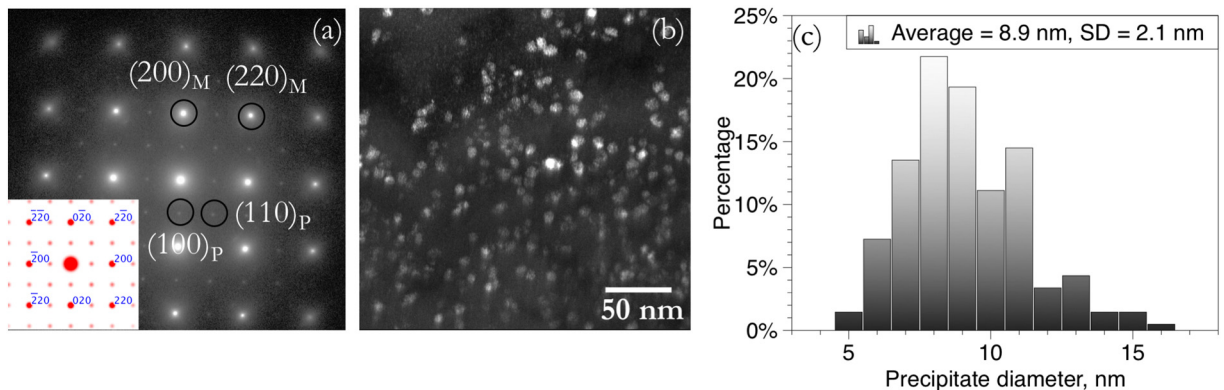


**Fig. 3.** In Al<sub>0.12</sub>NiCoFeCr alloy, (a) [001] zone axis Selected Area Diffraction Pattern obtained from the irradiated region showing diffracting points originating from the matrix and Ni<sub>3</sub>Al (L1<sub>2</sub>) type intermetallic precipitate phase, noted with subscripts M and P respectively. The inset shows the simulated [001] zone axis diffraction pattern of Ni<sub>3</sub>Al precipitate. (b) Dark field image obtained by keeping the objective aperture on the (100)<sub>P</sub> diffraction point showing the precipitates in bright contrast. (c) The size distribution of the precipitates in the irradiated region.

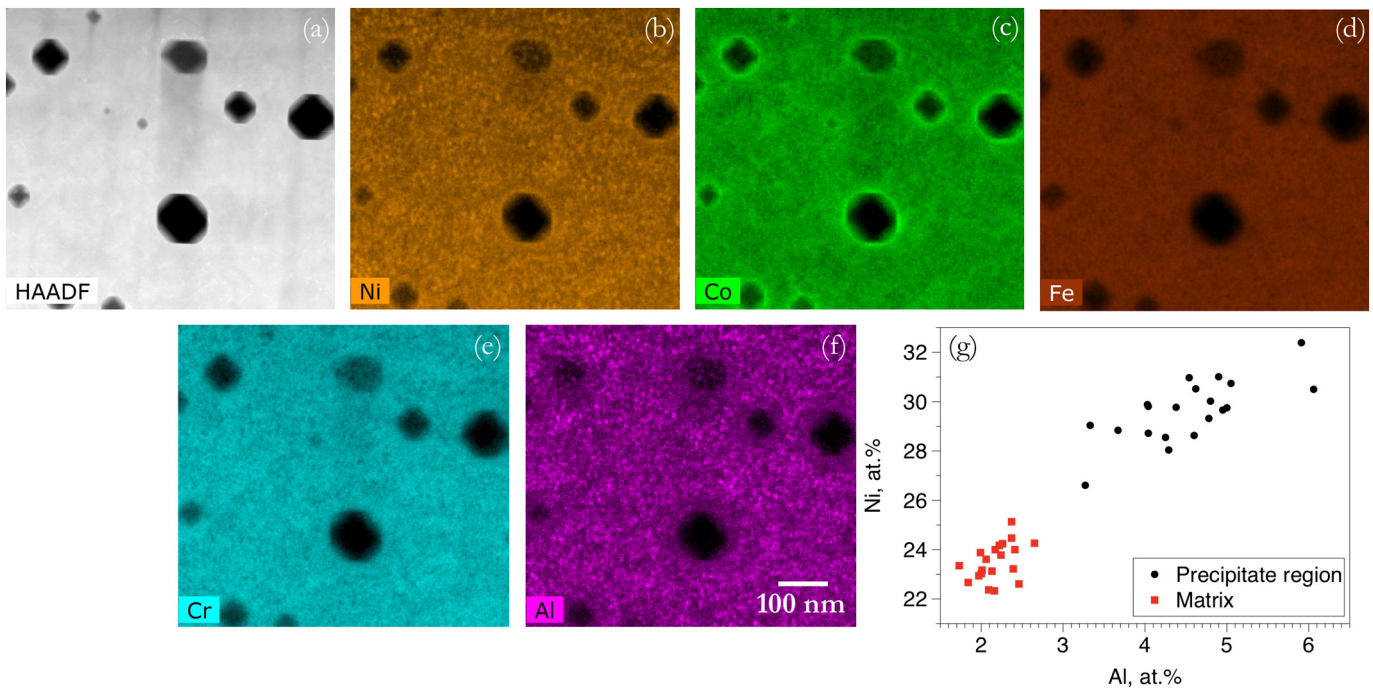


**Fig. 4.** In  $\text{Al}_{0.12}\text{NiCoFeCr}$  alloy, (a) STEM-HAADF image showing voids in the irradiation depth range of 0.2–0.9  $\mu\text{m}$  corresponding to the dose range of 45–100 dpa, (b–f) EDS count maps of elements Ni, Co, Fe, Cr and Al, (g) compositions extracted from the precipitate and the matrix regions. The scale bar in (f) is applicable to (a–f).

of the HEAs clearly showed that the solid solution of Al added alloy was unstable by forming the second phase under the irradiation conditions, while the solid solution of NiCoFeCr alloy exhibited stability. To discuss

the question how the irradiation resulted in precipitation in the Al added HEA, various mechanisms as found in different materials could be considered. As an assumption, a second phase is produced in a

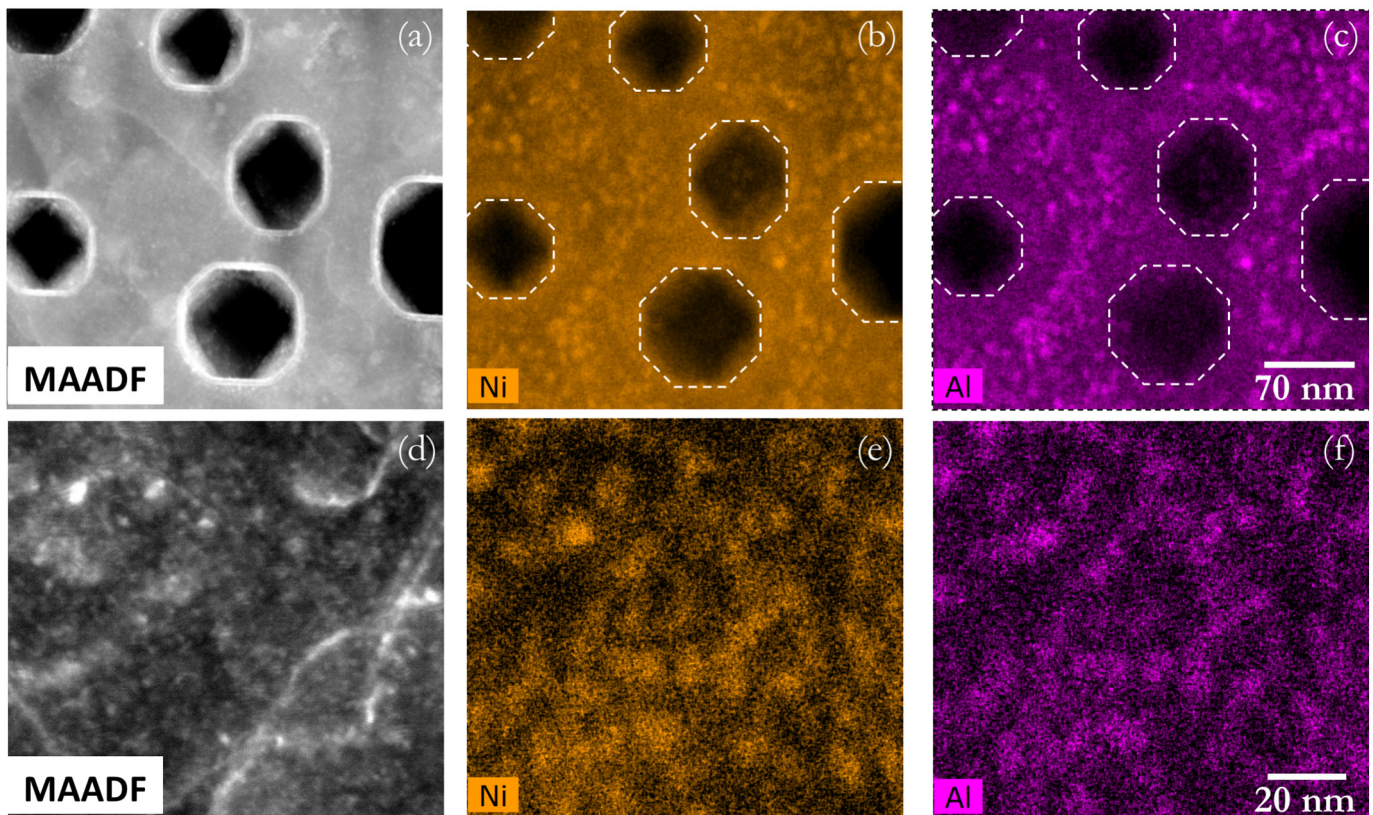


**Fig. 5.** (a) STEM-MAADF image  $\text{Al}_{0.12}\text{NiCoFeCr}$  HEA showing voids in the irradiation depth range of 0.3–0.6  $\mu\text{m}$  corresponding to the dose range of ~60–80 dpa, (b–c) EDS-Count maps exhibiting precipitates comprising of mainly Ni and Al. The dotted octagons on this image denotes the boundaries of the voids. Denuded zones of precipitates around the voids are visible. The scale bar in (c) is applicable to (a–c). (d) High magnification STEM-MAADF image and its EDS-count maps are given in (e–f) showing the enrichment of Ni and Al at the precipitates. The scale bar in (f) is applicable to (d–e).

single-phase region of alloys at the sinks where the amount of a constituent participating in the precipitation exceeds its solubility limit due to RIS. This possibility can be negated in our case since the precipitation in the Al-added HEA was observed in regions away from the voids with a homogenous distribution, whereas RIS could be found to occur only at voids and dislocation loops. Moreover, Al has been observed to deplete at the sinks, which doesn't help in rising up its level above the solubility limit [37].

The formation of the second phase during irradiation can be classified into two broad categories: RIP and radiation-enhanced precipitation (REP) as described in the introduction section. To understand which mechanism between them play a prominent role in precipitating the Ni-Al based intermetallic phase in the Al-added HEA, it is necessary to have the knowledge of the phase stability of the HEAs studied here at a given temperature. Among the several indicators for predicting stable solid solution formation in HEAs postulated in various studies, King et al. have identified two parameters named as,  $\delta$  and  $\Phi$ , that could correctly predict the stability of single phase in 177 alloy systems out of 185 alloy systems that have been experimentally verified [46]. Here,  $\delta$ , which estimates the difference in atomic radii, was calculated using the proceeding formulism as proposed by Ying et al. [47],

$$\delta = \sqrt{\sum_{i=1}^n c_i \left(1 - \frac{r_i}{\bar{r}}\right)^2} \times 100 \quad (1)$$

where,  $c_i$  is the concentration of element  $i$ ,  $r$  is the Goldschmit atomic radius of element  $i$  and  $\bar{r}$  is the weighted average of the systems atomic radii.

The second parameter,  $\Phi$ , is defined by King et al. as [46],

$$\Phi = \frac{\Delta G_{ss}}{-|\Delta G_{max}|} \quad (2)$$

where,  $\Delta G_{ss}$  is the Gibbs free energy for the formation of disordered solid solution from the mixture of the constituents of the alloy and  $\Delta G_{max}$  is the lowest possible Gibbs free energy obtainable from the formation of binary systems from the mixture of the constituents of the alloy. The change in the Gibbs free energy ( $\Delta G$ ) terms are calculated using the equation,

$$\Delta G = \Delta H - T\Delta S \quad (3)$$

In this equation, for calculating the  $\Delta G$  for the formation of solid solution and binary systems, the enthalpy of mixing of solid solution,  $\Delta H_{ss}$ , and intermetallic,  $\Delta H_{int}$ , are respectively substituted.  $T$  is assumed to be the melting temperature obtained using the rule of mixture. Only the configurational entropy change is considered in the calculation of  $\Delta G$ . More equations and details for the calculation of  $\Phi$  parameter can be obtained from the article by King et al. [46].

To form a stable solid solution at the melting temperature, it has been found empirically that the values of  $\delta$  and  $\Phi$  would have to be  $\leq 6.6$  and  $\geq 1$ , respectively, for the chosen constituents of the alloy [46,47]. These parametric values signify that the constituents would form disordered solid solution only when the atomic size difference among the elements is lower than a critical value and the Gibbs free energy for forming solid solution should exceed the lowest Gibbs free

energy to form an intermetallic out of the given constituents. Therefore, a negative value of  $\Phi$  would indicate that the constituents of the mixture do not form a stable solid solution at the melting temperature.

These values of  $\delta$  and  $\Phi$  along with the other relevant thermodynamic parameters for the HEAs studied here as calculated using the Alloy Search and Predict tool provided by King et al. are given in Table 1 [46]. While the values of  $\delta$  for both the NiCoFeCr and  $Al_{0.12}NiCoFeCr$  alloys were calculated to be 1.2 and 2.6, respectively, much lesser than 6.6, suggesting stable solid solution would form in these alloy systems, the values of  $\Phi$  points out that the NiCoFeCr alloy with the higher  $\Phi$  value (1.2) would be more stable as solid solution than the alloy with Al ( $\Phi = 0.9$ ). Furthermore, as given in Table 1, in the Al-added HEA, the elements Al and Ni have the lowest  $H_{max}$  – the maximum magnitude of the enthalpy of mixing for intermetallic formation – suggesting that Al-Ni based intermetallic can has the largest thermodynamic driving force to precipitate out in this alloy. Similarly, in the case of NiCoFeCr base alloy, intermetallic phase mainly composed of Cr and Ni has the highest chance for precipitating among all the possible intermetallic phases in this alloy at the melting temperature, but it has a higher maximum enthalpy of formation ( $H_{max} = -20$  kJ/mol) than the AlNi intermetallic in the Al added HEA ( $H_{max} = -29$  kJ/mol). Consistent with these observations, the phase diagram calculated for  $Al_{0.10}NiCoFeCr$  alloy using PanHEA database predicts the presence of 12% of  $L1_2$  phase coexisting with 15% of BCC phase, 50% of FCC phase and 22% of a sigma phase at 500 °C under the equilibrium condition [12]. Similarly,  $Al_{0.30}NiCoFeCr$  alloy, which has a higher Al content and was aged for 700 °C and 72 h was examined to have FCC A1 phase and FCC  $L1_2$  phase using experiments [39]. Interestingly, the measured volume fraction of the Ni-Al based second phase in the irradiated region, 9%, by assuming the thickness of the TEM specimen is 100 nm, is comparable to the one predicted by the phase diagram, 12%. Indeed, if the estimation of 100 nm TEM foil thickness is larger than the actual thickness, the volume fraction of Ni-Al second phases observed is likely to be an underestimation pushing the true value closer to the phase diagram value.

While the accuracies of these calculations based on the thermodynamic databases of all the phase in a system are unverified experimentally, they still indicate the existence of  $L1_2$  phase in the  $Al_{0.12}NiCoFeCr$  alloy under equilibrium at 500 °C. Therefore, we could argue that the radiation-enhanced diffusion enabled the precipitation of Ni-Al based intermetallic during irradiation due to the excessive point defects produced during the damage cascade on the top of thermal vacancies [48,49]. This argument is consistent with the observation that the non-irradiated region in the TEM specimen that had undergone similar thermal treatment as of the irradiated region had no precipitates. It clearly shows that the kinetics of the diffusion process proceeding at 500 °C for the irradiation time of 10 h was inadequate to bring the Ni-Al based intermetallic equilibrium phase out of the non-equilibrium phase.

To verify whether the Ni-Al intermetallic phase can precipitate during more extended ageing at 500 °C, the as-cast  $Al_{0.12}NiCoFeCr$  alloy was aged at 500 °C for 490 h. The chemical composition (in at. %) of the alloy as measured using STEM-EDS with the 3σ error is Ni -  $25.4 \pm 2.5$ , Co -  $24.6 \pm 2.4$ , Fe -  $24.1 \pm 2.3$ , Cr -  $22.6 \pm 2.0$  and Al -  $3.3 \pm 0.2$ . The alloy, however, still maintained the single phase after the ageing as observed by the SEM-EDS maps, diffraction pattern and TEM-EDS maps (Fig. 6), revealing its good phase stability under the thermal treatment. Particularly, the grain boundaries of the annealed alloy, where heterogeneous nucleation of second phases have been observed in certain HEAs, showed no precipitation as well [36]. Regardless, whether the Ni-Al intermetallic phase is an equilibrium phase in the alloy remains inconclusive from this ageing experiment, since it is possible that this phase could take a longer time to precipitate out at this temperature. This scenario is plausible considering that the diffusion kinetics in high entropy alloys has been shown to be sluggish owing to their compositional complexity, delaying the precipitation of the equilibrium phases.

**Table 1**

Thermodynamic parameters, utilized for the phase stability prediction, of the alloys investigated in this study [46].  $H_{max}$ : The maximum magnitude of the enthalpy of mixing for intermetallic/multiphase formation (kJ/mol); Elements AB: The binary mixture that yields the highest magnitude ( $H_{max}$ ).

System	$\delta$	$\Phi$	$H_{max}$ (kJ/mol)	Elements AB
NiCoFeCr	1.2	1.2	-20	CrNi
$Al_{0.12}NiCoFeCr$	2.6	0.9	-29	AlNi

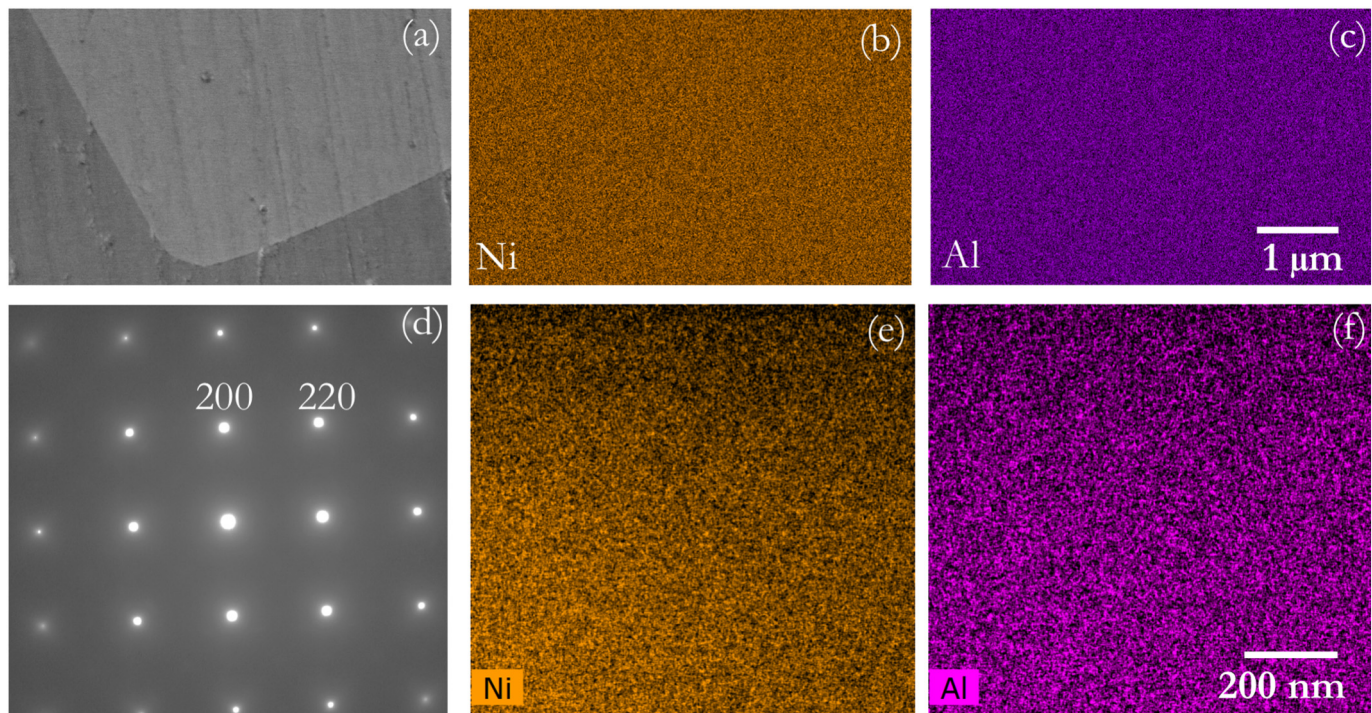


**Fig. 6.**  $\text{Al}_{0.12}\text{NiCoFeCr}$  aged for 490 h at 500 °C showing no second phase formation. (a) Back scattering electron image revealing a grain boundary, (b) and (c) SEM-EDS count maps of elements Ni and Al obtained from the same location as (a). The scale bar in (c) is applicable to (a–b). (d) Diffraction pattern recorded from its TEM specimen showing no diffraction points from any second phase, (e) and (f) STEM-EDS count maps of elements Ni and Al. The scale bar in (f) is applicable to (e–f).

Interestingly, Shun and Du found nanoprecipitates rich in Ni and Al with  $\text{L1}_2$  ordered structure in as cast  $\text{Al}_{0.3}\text{NiCoFeCr}$ , suggesting that such phases could be an equilibrium phase in  $\text{Al}_{0.1}\text{NiCoFeCr}$  alloy as well [50]. Furthermore, several studies showed that prolonged annealing times are needed to bring the equilibrium phases out of the solid solution in high entropy alloys. For instance, in  $\text{CrMnFeCoNi}$  single phase alloy, Pickering et al. observed  $\text{M}_{23}\text{C}_6$  phase and a Cr-rich  $\sigma$ -phase after annealing for 500 h – 1000 h at 700 °C and Otto et al. performed annealing at the temperature range of 500 to 900 °C for 500 days to observed to more complex phases, though, in this case, the time at which the decomposition has started was not known [36,50,51].

Based on the discussions, we suggest that the precipitates formed in the irradiated region were produced heterogeneously by the radiation-enhanced diffusion. Irradiation produces a greater concentration of vacancies and interstitials than what is generated thermally and therefore enhances the diffusion coefficients of the defects in the material [48,52]. Several studies have attempted to calculate the enhancement in the diffusion coefficient under irradiation. For instance, Dienes and Damask found that the difference between the normal diffusion coefficient and the radiation-induced diffusion coefficient is proportional to the square root of the radiation flux with a lower activation energy of  $\frac{1}{2}E_m^V$ , where  $E_m^V$  is the vacancy migration energy under the steady state conditions [53]. By irradiating brass specimens at temperatures up to 190 °C and measuring the electrical resistivity at the liquid nitrogen temperature, they also estimated the diffusion coefficient to be much higher than the normal diffusion coefficient [53]. Also, the difference in the diffusion coefficient was measured to be higher at low irradiation temperatures since the proportion of radiation-induced point defects is significantly larger than the thermally produced vacancy concentration. Similarly, radiation-enhanced diffusion has been observed in several material systems such as amorphous Si, Ge, MgO, NiSi alloys [21,22,54–57]. Furthermore, the contribution of radiation-enhanced diffusion in precipitation is supported by our experimental observation of precipitate-denuded zones extending typically for 40 nm from the edges of the voids. Formation of such zones can be ascribed to the

insufficient diffusion kinetics in the region close to sinks, where the vacancy concentration can be approximated to the equilibrium thermal vacancy concentration owing to excess vacancy absorption [58,59]. In other words, the regions surrounding the voids behaved similar to the non-irradiated region of the sample, where no precipitates formed.

The findings of this study underscore that even single-phase high entropy alloys, such as  $\text{Al}_{0.12}\text{NiCoFeCr}$ , which could retain its phase stability during the lengthy thermal treatments, could decompose into multiple phases including intermetallic phase rapidly with the assistance from irradiation. It would be interesting to examine whether how the  $\text{Ni}_3\text{Al}$  type precipitates affect the chemical and mechanical properties of the original HEA. From the literature, we could point out that the  $\text{Ni}_3\text{Al}$  type precipitates formed in the Ni-base superalloys and Fe-Cr-Al alloys have increased the strength and toughness of the materials [60,61]. Similarly,  $\text{NiAl}$  type precipitates with B2 phase produced during welding in the  $\text{CoCrFeNiMn}$  HEA was measured to increase the hardness of the alloy [62]. On the other hand, it is plausible that such intermetallic phase formation in HEAs, if continue evolving, during service in a harsh radiation environment could endanger the structural integrity of the components through precipitous loss in ductility or corrosion resistance. Therefore, while high entropy alloys provide attractive properties for applications in a radiation environment, our study clearly shows that their phase stability under irradiation should be considered as one of the deciding factors in the materials selection for such applications.

## 5. Conclusions

Phase stability of equiatomic and Al doped single phase high entropy alloys,  $\text{NiCoFeCr}$  and  $\text{Al}_{0.12}\text{NiCoFeCr}$ , was studied under 3 MeV  $\text{Ni}^{2+}$  irradiation at 500 °C to a fluence of  $1 \times 10^{17}/\text{cm}^2$  reaching a peak dose of ~100 dpa at about 1 μm depth. TEM diffraction pattern and STEM-EDS were utilized to detect any second phases that formed in the irradiated regions of the specimens. While the single phase of  $\text{NiCoFeCr}$  alloy has

remained stable under the irradiation, the  $\text{Al}_{0.12}\text{NiCoFeCr}$  alloy decomposed into FCC matrix phase and  $\text{Ni}_3\text{Al}$  type nanoprecipitates with  $\text{L1}_2$  ordered structure. The average size of the precipitates was 9 nm, and their volume fraction was estimated to be 9%. No precipitates, however, were found in the non-irradiated region of the TEM specimen, which had undergone similar heat treatment as that of the irradiated region. Precipitate-denuded zones were noted around the radiation-produced voids.

To verify whether the  $\text{Ni}_3\text{Al}$  type phase is an equilibrium phase in the  $\text{Al}_{0.12}\text{NiCoFeCr}$  alloy system, its as-cast sample was annealed at 500 °C for 490 h to allow more time at the irradiation temperature for the system to reach the equilibrium. Like the non-irradiated region, however, the alloy maintained its single phase even after the long annealing treatment. Nevertheless, thermodynamic indicators for phase stability point out that  $\text{Al}_{0.12}\text{NiCoFeCr}$  is less stable than  $\text{NiCoFeCr}$ . In the former one, the Ni and Al have the maximum enthalpy of mixing for intermetallic formation ( $-29 \text{ kJ/mol}$ ), suggesting the formation of  $\text{NiAl}$  intermetallic has the highest driving force among all the possible binary combinations.

Based upon the results, we propose that the physical mechanism behind the formation of these precipitates is radiation-enhanced non-equilibrium diffusion process that drives diffusion kinetics out of solid solution to form the second phases, accelerates the precipitate formation in comparison to equilibrium thermal treatment. Such phase transformation during service in radiation environment could endanger the structural integrity of the components through precipitous loss in ductility or corrosion resistance. Therefore, our study clearly shows that the phase stability of high entropy alloys under irradiation should be considered as one of the deciding factors in the materials selection for nuclear applications.

### CRediT authorship contribution statement

**B. Kombaiah:** Formal analysis, Writing - original draft, Writing - review & editing. **K. Jin:** Writing - review & editing. **H. Bei:** Writing - review & editing. **P.D. Edmondson:** Writing - review & editing. **Y. Zhang:** Writing - review & editing.

### Acknowledgements

This work was supported as part of the Energy Dissipation to Defect Evolution (EDDE), an Energy Frontier Research Center funded by the U.S. Department of Energy, Office of Science, Basic Energy Sciences under contract number DE-AC05-00OR22725. Some microstructure characterizations were performed using instrumentation (Talos F200X) provided by the Department of Energy, Office of Nuclear Energy, Fuel Cycle R&D Program and the Nuclear Science User Facilities. BK acknowledges Drs. Ying Yang, Easo George and Steve Zinkle of Materials Science and Technology Division of Oak Ridge National Laboratory for the valuable discussions.

### Author contributions

B.K. contributed to conceptualization, methodology, data curation, formal analysis, investigation, visualization and writing - original draft. K.J. contributed to conceptualization and methodology. H.B. contributed to methodology. P.E. contributed to investigation, methodology, supervision and validation. Y.Z. contributed to conceptualization, funding acquisition, investigation, methodology, project administration, supervision, and validation. All contributed to writing - review & editing.

### Data availability

The raw data required to reproduce these findings are available to download from <http://dx.doi.org/10.17632/xm7xpz8ykj.1>.

### References

- [1] High-entropy Alloys: Fundamentals and Applications., Springer, Switzerland, 2016.
- [2] B. Gludovatz, A. Hohenwarter, D. Catoor, E.H. Chang, E.P. George, R.O. Ritchie, A fracture-resistant high-entropy alloy for cryogenic applications, *Science* 345 (6201) (2014) 1153–1158.
- [3] N. Kumar, M. Komarasamy, P. Nelaturu, Z. Tang, P.K. Liaw, R.S. Mishra, Friction stir processing of a high entropy alloy  $\text{Al}_{0.1}\text{CoCrFeNi}$ , *JOM* 67 (5) (2015) 1007–1013.
- [4] C.P. Lee, C.C. Chang, Y.Y. Chen, J.W. Yeh, H.C. Shih, Effect of the aluminium content of  $\text{Al}_{x}\text{CrFe}_{1.5}\text{MnNi}_{0.5}$  high-entropy alloys on the corrosion behaviour in aqueous environments, *Corros. Sci.* 50 (7) (2008) 2053–2060.
- [5] D.H. Xiao, P.F. Zhou, W.Q. Wu, H.Y. Diao, M.C. Gao, M. Song, P.K. Liaw, Microstructure, mechanical and corrosion behaviors of  $\text{AlCoCuFeNi-(Cr,Ti)}$  high entropy alloys, *Mater. Des.* 116 (2017) 438–447.
- [6] A. Zhang, J. Han, B. Su, P. Li, J. Meng, Microstructure, mechanical properties and tribological performance of  $\text{CoCrFeNi}$  high entropy alloy matrix self-lubricating composite, *Mater. Des.* 114 (2017) 253–263.
- [7] Y. Zhang, G.M. Stocks, K. Jin, C. Lu, H. Bei, B.C. Sales, L. Wang, L.K. Beland, R.E. Stoller, G.D. Samolyuk, M. Caro, A. Caro, W.J. Weber, Influence of chemical disorder on energy dissipation and defect evolution in concentrated solid solution alloys, *Nat. Commun.* 6 (2015) 8736.
- [8] C. Lu, L. Niu, N. Chen, K. Jin, T. Yang, P. Xiu, Y. Zhang, F. Gao, H. Bei, S. Shi, M.R. He, I.M. Robertson, W.J. Weber, L. Wang, Enhancing radiation tolerance by controlling defect mobility and migration pathways in multicomponent single-phase alloys, *Nat. Commun.* 7 (2016) 13564..
- [9] K. Jin, C. Lu, L.M. Wang, J. Qu, W.J. Weber, Y. Zhang, H. Bei, Effects of compositional complexity on the ion-irradiation induced swelling and hardening in Ni-containing equiatomic alloys, *Scr. Mater.* 119 (2016) 65–70.
- [10] Y. Zhang, S. Zhao, W.J. Weber, K. Nordlund, F. Granberg, F. Djurabekova, Atomic-level heterogeneity and defect dynamics in concentrated solid-solution alloys, *Curr. Opin. Solid State Mater. Sci.* 21 (5) (2017) 221–237.
- [11] R.S. Mishra, N. Kumar, M. Komarasamy, Lattice strain framework for plastic deformation in complex concentrated alloys including high entropy alloys, *Mater. Sci. Technol.* 31 (10) (2015) 1259–1263.
- [12] S. Xia, M.C. Gao, T. Yang, P.K. Liaw, Y. Zhang, Phase stability and microstructures of high entropy alloys ion irradiated to high doses, *J. Nucl. Mater.* 480 (2016) 100–108.
- [13] K.L. Murty, I. Chait, Structural materials for Gen-IV nuclear reactors: challenges and opportunities, *J. Nucl. Mater.* 383 (1–2) (2008) 189–195.
- [14] S.J. Zinkle, G.S. Was, Materials challenges in nuclear energy, *Acta Mater.* 61 (3) (2013) 735–758.
- [15] T. Egami, W. Guo, P.D. Rack, T. Nagase, Irradiation resistance of multicomponent alloys, *Metall. Mater. Trans. A* 45 (1) (2013) 180–183.
- [16] M. Bachhav, G. Robert Odette, E.A. Marquis,  $\alpha'$  precipitation in neutron-irradiated Fe-Cr alloys, *Scr. Mater.* 74 (2014) 48–51.
- [17] K.G. Field, K.C. Littrell, S.A. Briggs, Precipitation of  $\alpha'$  in neutron irradiated commercial  $\text{FeCrAl}$  alloys, *Scr. Mater.* 142 (2018) 41–45.
- [18] M.H. Mathon, Y. de Carlan, G. Geoffroy, X. Avery, A. Alamo, C.H. de Novion, A SANS investigation of the irradiation-enhanced  $\alpha-\alpha'$  phases separation in 7–12 Cr martensitic steels, *J. Nucl. Mater.* 312 (2–3) (2003) 236–248.
- [19] H.R. Brager, F.A. Garner, Swelling as a consequence of gamma prime ( $\gamma'$ ) and M23 (C, Si)<sub>6</sub> formation in neutron irradiated 316 stainless steel, *J. Nucl. Mater.* 73 (1) (1978) 9–19.
- [20] Z. Jiao, G.S. Was, Novel features of radiation-induced segregation and radiation-induced precipitation in austenitic stainless steels, *Acta Mater.* 59 (3) (2011) 1220–1238.
- [21] A. Barbu, A.J. Ardell, Irradiation-induced precipitation in Ni-Si alloys, *Scr. Metall.* 9 (11) (1975) 1233–1237.
- [22] A. Barbu, G. Martin, Radiation induced precipitation in nickel silicon solid solutions: dose rate effects, *Scr. Metall.* 11 (9) (1977) 771–775.
- [23] P.D. Edmondson, M.K. Miller, K.A. Powers, R.K. Nanstad, Atom probe tomography characterization of neutron irradiated surveillance samples from the R. E. Ginna reactor pressure vessel, *J. Nucl. Mater.* 470 (2016) 147–154.
- [24] H. Ke, P. Wells, P.D. Edmondson, N. Almirall, L. Barnard, G.R. Odette, D. Morgan, Thermodynamic and kinetic modeling of Mn-Ni-Si precipitates in low-Cu reactor pressure vessel steels, *Acta Mater.* 138 (2017) 10–26.
- [25] R. Cauvin, G. Martin, Radiation induced homogeneous precipitation in undersaturated solid-solutions, *J. Nucl. Mater.* 83 (1) (1979) 67–78.
- [26] R. Cauvin, G. Martin, Solid solutions under irradiation. II. Radiation-induced precipitation in  $\text{AlZn}$  undersaturated solid solutions, *Phys. Rev. B* 23 (7) (1981) 3333–3348.
- [27] R. Cauvin, G. Martin, Solid solutions under irradiation. I. A model for radiation-induced metastability, *Phys. Rev. B* 23 (7) (1981) 3322–3332.
- [28] S. Ranganathan, Alloyed pleasures – multimetallic cocktails, *Curr. Sci.* 85 (10) (2003) 1404–1406.
- [29] J.W. Yeh, S.K. Chen, S.J. Lin, J.Y. Gan, T.S. Chin, T.T. Shun, C.H. Tsau, S.Y. Chang, Nanostructured high-entropy alloys with multiple principal elements: novel alloy design concepts and outcomes, *Adv. Eng. Mater.* 6 (5) (2004) 299–303.
- [30] B. Schuh, F. Mendez-Martin, B. Volker, E.P. George, H. Clemens, R. Pippan, A. Hohenwarter, Mechanical properties, microstructure and thermal stability of a nanocrystalline  $\text{CoCrFeMnNi}$  high-entropy alloy after severe plastic deformation, *Acta Mater.* 96 (2015) 258–268.
- [31] C.-M. Lin, H.-L. Tsai, Evolution of microstructure, hardness, and corrosion properties of high-entropy  $\text{Al}_{0.5}\text{CoCrFeNi}$  alloy, *Intermetallics* 19 (3) (2011) 288–294.
- [32] N.A.P.K. Kumar, C. Li, K.J. Leonard, H. Bei, S.J. Zinkle, Microstructural stability and mechanical behavior of  $\text{FeNiMnCr}$  high entropy alloy under ion irradiation, *Acta Mater.* 113 (2016) 230–244.

- [33] T. Yang, S. Xia, S. Liu, C. Wang, S. Liu, Y. Fang, Y. Zhang, J. Xue, S. Yan, Y. Wang, Precipitation behavior of Al<sub>x</sub>CoCrFeNi high entropy alloys under ion irradiation, *Sci. Rep.* 6 (2016), 32146.
- [34] M.-R. He, S. Wang, S. Shi, K. Jin, H. Bei, K. Yasuda, S. Matsumura, K. Higashida, I.M. Robertson, Mechanisms of radiation-induced segregation in CrFeCoNi-based single-phase concentrated solid solution alloys, *Acta Mater.* 126 (2017) 182–193.
- [35] C. Lu, T. Yang, K. Jin, N. Gao, P. Xiu, Y. Zhang, F. Gao, H. Bei, W.J. Weber, K. Sun, Y. Dong, L. Wang, Radiation-induced segregation on defect clusters in single-phase concentrated solid-solution alloys, *Acta Mater.* 127 (2017) 98–107.
- [36] F. Otto, A. Dlouhý, K.G. Pradeep, M. Kuběnová, D. Raabe, G. Eggeler, E.P. George, Decomposition of the single-phase high-entropy alloy CrMnFeCoNi after prolonged anneals at intermediate temperatures, *Acta Mater.* 112 (2016) 40–52.
- [37] T. Yang, S. Xia, W. Guo, R. Hu, J.D. Poplawsky, G. Sha, Y. Fang, Z. Yan, C. Wang, C. Li, Y. Zhang, S.J. Zinkle, Y. Wang, Effects of temperature on the irradiation responses of Al<sub>0.1</sub>CoCrFeNi high entropy alloy, *Scr. Mater.* 144 (2018) 31–35.
- [38] S.Q. Xia, X. Yang, T.F. Yang, S. Liu, Y. Zhang, Irradiation resistance in Al<sub>x</sub>CoCrFeNi high entropy alloys, *JOM* 67 (10) (2015) 2340–2344.
- [39] C. Zhang, F. Zhang, H. Diao, M.C. Gao, Z. Tang, J.D. Poplawsky, P.K. Liaw, Understanding phase stability of Al-Co-Cr-Fe-Ni high entropy alloys, *Mater. Des.* 109 (2016) 425–433.
- [40] W.-R. Wang, W.-L. Wang, S.-C. Wang, Y.-C. Tsai, C.-H. Lai, J.-W. Yeh, Effects of Al addition on the microstructure and mechanical property of Al<sub>x</sub>CoCrFeNi high-entropy alloys, *Intermetallics* 26 (2012) 44–51.
- [41] S.J. Zinkle, J.T. Busby, Structural materials for fission & fusion energy, *Mater. Today* 12 (11) (2009) 12–19.
- [42] Y. Zhang, M.L. Crespillo, H. Xue, K. Jin, C.H. Chen, C.L. Fontana, J.T. Graham, W.J. Weber, New ion beam materials laboratory for materials modification and irradiation effects research, *Nucl. Instrum. Methods Phys. Res., Sect. B* 338 (2014) 19–30.
- [43] R.E. Stoller, M.B. Toloczko, G.S. Was, A.G. Certain, S. Dwarkarnath, F.A. Garner, On the use of SRIM for computing radiation damage exposure, *Nucl. Instrum. Methods Phys. Res., Sect. B* 310 (2013) 75–80.
- [44] J.F. Ziegler, M.D. Ziegler, J.P. Biersack, SRIM – the stopping and range of ions in matter (2010), *Nucl. Instrum. Methods Phys. Res., Sect. B* 268 (11) (2010) 1818–1823.
- [45] G.W. Lorimer, Quantitative X-ray microanalysis of thin specimens in the transmission electron microscope; a review, *Mineral. Mag.* 51 (1987) 49–60.
- [46] D.J.M. King, S.C. Middleburgh, A.G. McGregor, M.B. Cortie, Predicting the formation and stability of single phase high-entropy alloys, *Acta Mater.* 104 (2016) 172–179.
- [47] X. Yang, Y. Zhang, Prediction of high-entropy stabilized solid-solution in multi-component alloys, *Mater. Chem. Phys.* 132 (2–3) (2012) 233–238.
- [48] T.R. Allen, G.S. Was, *Radiation-enhanced Diffusion and Radiation-induced Segregation*, Springer Netherlands, Dordrecht, 2007 123–151.
- [49] R. Sizmann, The effect of radiation upon diffusion in metals, *J. Nucl. Mater.* 69–70 (1978) 386–412.
- [50] T.-T. Shun, Y.-C. Du, Microstructure and tensile behaviors of FCC Al<sub>0.3</sub>CoCrFeNi high entropy alloy, *J. Alloys Compd.* 479 (1–2) (2009) 157–160.
- [51] E.J. Pickering, R. Muñoz-Moreno, H.J. Stone, N.G. Jones, Precipitation in the equiatomic high-entropy alloy CrMnFeCoNi, *Scr. Mater.* 113 (2016) 106–109.
- [52] G.S. Was, *Fundamentals of Radiation Materials Science: Metals and Alloys*, Springer, New York, 2007.
- [53] G.J. Dienes, A.C. Damask, Radiation enhanced diffusion in solids, *J. Appl. Phys.* 29 (12) (1958) 1713–1721.
- [54] F. Priolo, J.M. Poate, D.C. Jacobson, J. Linnros, J.L. Batstone, S.U. Campisano, Radiation-enhanced diffusion of Au in amorphous Si, *Appl. Phys. Lett.* 52 (15) (1988) 1213–1215.
- [55] R.L. Minear, D.G. Nelson, J.F. Gibbons, Enhanced diffusion in Si and Ge by light ion implantation, *J. Appl. Phys.* 43 (8) (1972) 3468–3480.
- [56] A.I.V. Sambeek, R.S. Averback, C.P. Flynn, M.H. Yang, W. Jäger, Radiation enhanced diffusion in MgO, *J. Appl. Phys.* 83 (12) (1998) 7576–7584.
- [57] G. Martin, Phase stability under irradiation: ballistic effects, *Phys. Rev. B* 30 (3) (1984) 1424–1436.
- [58] L.K. Mansur, Void swelling in metals and alloys under irradiation: an assessment of the theory, *Nucl. Technol.* 40 (1) (1978) 5–34.
- [59] B.N. Singh, D.J. Edwards, M. Eldrup, P. Toft, Effects of heat treatments and neutron irradiation on microstructures and physical and mechanical properties of copper alloys, *J. Nucl. Mater.* 249 (1) (1997) 1–16.
- [60] T.M. Pollock, S. Tin, Nickel-based superalloys for advanced turbine engines: chemistry, microstructure and properties, *J. Propuls. Power* 22 (2) (2006) 361–374.
- [61] R. Moskovic, Mechanical properties of precipitation-strengthened Ni-Al-Cr alloy based on an NiAl intermetallic compound, *J. Mater. Sci.* 13 (9) (1978) 1901–1906.
- [62] N. Kashaev, V. Ventzke, N. Stepanov, D. Shaysultanov, V. Sanin, S. Zherebtsov, Laser beam welding of a CoCrFeNiMn-type high entropy alloy produced by self-propagating high-temperature synthesis, *Intermetallics* 96 (2018) 63–71.